Copper storage protein from *Streptomyces lividans*

Jonathan AR Worrall

School of Life Sciences, University of Essex, Wivenhoe Park, Colchester, UK

FUNCTIONAL CLASS

Protein; widespread in bacteria; multicuprous ion-binding sites; referred to as copper storage protein.

Bacterial copper storage proteins (Csps) belong to the DUF326 superfamily (PF03860) (DUF domain of unknown function) that contain a cysteine-rich repeat that mostly follows the pattern Cys-X_2-Cys-X_3-Cys-X_2-Cys-X. Their functional state comprises a homotetramer assembly of four-helix bundle motifs. Depending on their cellular location, that is periplasmic or cytosolic, they have the capacity to bind between 13 and 20 cuprous ions per four-helix bundle (52–80 cuprous ions per homotetramer) predominantly through thiolate coordination chemistry. Their apparent Cu^I-binding affinities are in the subfemtomolar range.

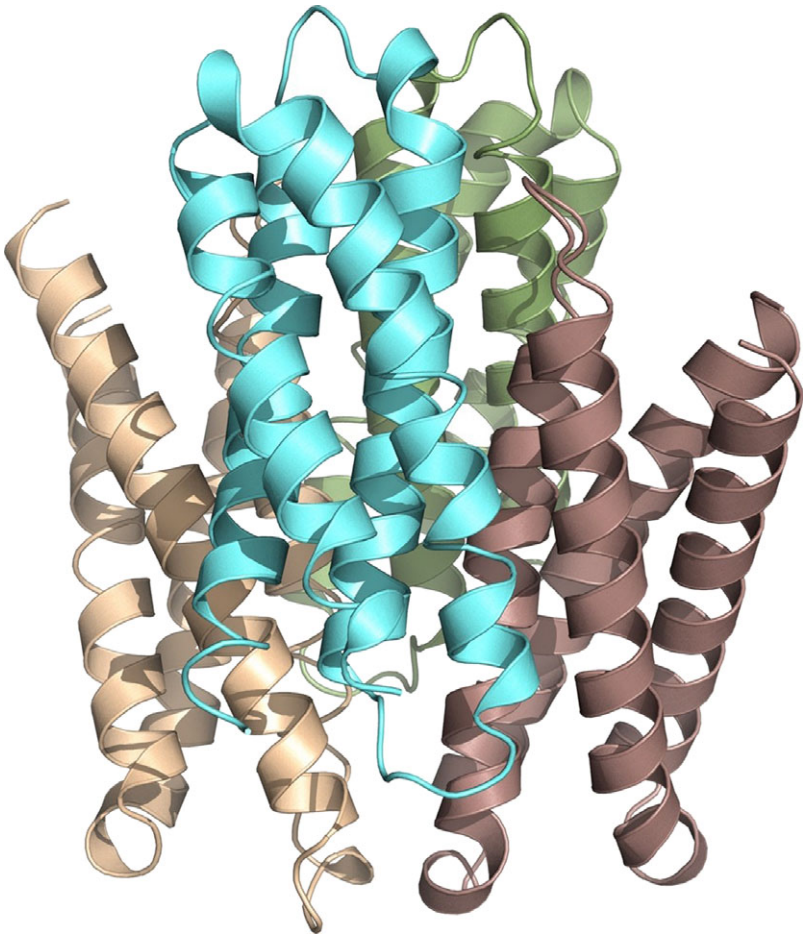

3D Structure Cartoon representation of the homotetramer assembly of the copper storage protein form *Streptomyces lividans*, PDB code: 6EI0.[1] Each four-helix bundle (protomer) of the functional assembly is individually colored. [Based on ML Straw, AK Chaplin, MA Hough, J Paps, VN Bavro, MT Wilson, E Vijgenboom, JAR Worrall, *Metallomics*, **10**, 180–193 (2018).]

Encyclopedia of Inorganic and Bioinorganic Chemistry, Online © 2011–2021 John Wiley & Sons, Ltd.

This article was published in the *Encyclopedia of Inorganic and Bioinorganic Chemistry* in 2021 by John Wiley & Sons, Ltd.
DOI: 10.1002/9781119951438.eibc2777

OCCURRENCE

Csps were first discovered in the Gram-negative methane-oxidizing bacterium, *Methylosinus trichosporium* OB3b.[2] Two Csps, initially named Csp1 and Csp2, were found to contain a twin-arginine translocase (Tat) signal peptide, signifying their export to the periplasm in a folded state. A third Csp, not possessing a Tat signal peptide, was also identified in *M. trichosporium* OB3b and named Csp3.[2] The absence of a Tat signal peptide implies that Csp3 is not exported and remains in the cytosol. *M. trichosporium* OB3b Csp1 and Csp2 were later renamed Csp1a and 1b, respectively, to signify exported Csps homologues with a similar function.[3] The taxonomic distribution of Csp3s reveals them to be more widespread in bacteria than the Csp1 homologues.[1–3] At least seven Bacterial groups contain Csp3, and they are also found within two of the major Archaea groups.[1] Recombinant Csp1a and Csp3 from *M. trichosporium* OB3b have been purified and extensively characterized,[2,4] as have two Csp3 members from the non-methanotrophic Gram-positive bacteria, *Bacillus subtilis*[4] and *Streptomyces lividans*.[1] The latter (*Sl*Csp3) is the subject of this article.

BIOLOGICAL FUNCTION

Methanotrophic bacteria oxidize methane to CO_2 via methanol, formaldehyde, and formate. To catalyze the oxidation of methane to methanol either the membrane-bound particulate methane monooxygenase (pMMO) or soluble methane monooxygenase (sMMO) is used.[5,6] pMMO is located within extensive intracytoplasmic membranes and is a cuproenzyme (see ***Particulate Methane Monooxygenase***),[7–11] whereas sMMO is located in the cytoplasm and contains a diiron active site (see ***Methane Monooxygenase Hydroxylase***).[12,13] In organisms containing genes for both sMMO and pMMO, the regulation of sMMO is controlled by a mechanism referred to as the 'copper switch' whereby sMMO is expressed under low copper conditions, but under copper replete conditions is downregulated.[6,7,14–17] When methanotrophs use pMMO to oxidize methane it can account for up to 20% of the total protein content of the cell, and thus a significant requirement of copper is needed by the organism.[16–19] To cope with this large requirement for copper, small peptidic copper chelators, called methanobactins (Mbn), are secreted to scavenge for copper, with Cu-Mbn reinternalized into the methanotroph.[17,20–22] Metalloproteomic studies using the copper-switching organism *M. trichosporium* OB3b designed to determine the fate of the reinternalized Cu-Mbn surprisingly found no evidence for the presence of apo-Mbn or Cu-Mbn but instead identified soluble copper pools associated with the Tat-exported Csp1 homologues.[2] Several further lines of study concluded that Csp1s act as a Cu^{I} store for pMMO to maintain its use for methane metabolism under low copper levels.[2]

In contrast, the exact function of bacterial Csp3s remains under debate.[3,23] If not carefully regulated, Cu^{I} can be highly toxic in the reducing environment of the bacterial cytosol.[24] Based on the Irving–Williams series of metal-binding preferences,[25] copper and particularly Cu^{I} will readily displace or outcompete the cognate metal for a binding site, as has been exemplified for iron in Fe–S clusters,[26–29] leading to detrimental effects on the cell. For this reason, copper-specific bacterial regulatory systems are prevalent that act to rapidly efflux excess Cu^{I} out of the cytosol.[24,30] The presence of such systems has helped support the view that a metabolic requirement for cuproenzymes in the bacterial cytosol does not exist. However, with the discovery of Csp3s, it would appear that the handling of copper in the bacterial cytosol is perhaps more complicated, and elucidating their role in connection to preventing toxicity and/or in copper storage for metabolic use has been the subject of recent studies.[1,4,31]

DEPOSITED X-RAY STRUCTURES OF Csp3s IN THE PROTEIN DATA BANK

Several X-ray structures of Csp3 members have been deposited in the protein data bank (PDB), which include structures of apo and cuprous ion-loaded forms, structures of amino-acid variants, and structures determined following varying substoichiometric additions of cuprous ions (Table 1). Two of the deposited X-ray structures reported in Table 1, *Pseudomonas aeruginosa* Csp3 (*Pa*Csp3) and *Nitrosospira multiformis* Csp3 (*Nm*Csp3), were deposited to the PDB in 2009 and 2010, respectively, by the Northeast Structural Genomics Consortium (NESG). The deposition of these structures preceded the discovery and first report of the Csp family.[2]

AMINO ACID SEQUENCE INFORMATION

- *S. lividans* 1326, 136 amino acids, UniProtKB entry D6ES11, Q9X8F4
- *B. subtilis*, 108 amino acids, UniProtKB entry O07571, sequence identity with *Sl*Csp3 38%
- *P. aeruginosa*, 134 amino acids, UniProtKB entry Q91208, sequence identity with *Sl*Csp3 31%
- *N. multiformis*, 113 amino acids, UniProtKB entry Q2Y879, sequence identity with *Sl*Csp3 27%
- *M. trichosporium* OB3b, 133 amino acids, no UniProtKB entry, sequence identity with *Sl*Csp3 48%.

This article was published in the *Encyclopedia of Inorganic and Bioinorganic Chemistry* in 2021 by John Wiley & Sons, Ltd.
DOI: 10.1002/9781119951438.eibc2777

Table 1 X-ray crystal structures deposited in the PDB for various Csp3 members

Organism	PDB code and resolution	Description of structure deposited	Number of Cys residues per four-helix bundle
Streptomyces lividans (*Sl*Csp3)	6EI0, 1.34 Å	apo state	18
	6EK9, 1.50 Å	20 Cu^{I} ions bound	
	6QYB, 1.20 Å	H111A variant, 19 Cu^{I} ions bound	
	6QVH, 1.30 Å	H113A variant, 20 Cu^{I} ions bound	
	6R01, 1.20 Å	H107A/H111A variant, 19 Cu^{I} ions bound	
	6Q58, 1.50 Å	5 Cu^{I} equivalents added, partial occupancies	
	6Q6B, 1.90 Å	10 Cu^{I} equivalents added, partial occupancies	
Methylosinus trichosporium OB3b (*Mt*Csp3)	5ARM, 1.19 Å	apo state	19
	5ARN, 2.30 Å	19 Cu^{I} ions bound	
	5NQM, 1.59 Å	1–2 Cu^{I} equivalents added, partial occupancies	
	5NQN, 1.62 Å	8 Cu^{I} equivalents added, partial occupancies	
	5NQO, 1.15 Å	14 Cu^{I} equivalents added, partial occupancies	
Bacillus subtilis (*Bs*Csp3)	5FIG, 1.7 Å	apo state	19
Pseudomonas aeruginosa (*Pa*Csp3)	3KAW, 2.40 Å	apo state	12
	3KAV, 2.50 Å	L80M variant, apo state	
Nitrosospira multiformis (*Nm*Csp3)	3LMF, 2.30 Å	apo state	16

[Data available from the PDB (protein data bank).]

PROTEIN PRODUCTION AND PURIFICATION

A recombinant *Escherichia coli* overexpression system for *Sl*Csp3 has been reported,[1] which produces an N-terminal His_6-tagged *Sl*Csp3 fusion protein from a pET28a plasmid under the control of a T7 promoter. The overexpressed *Sl*Csp3 is subsequently purified using a high-pressure homogenizer to rupture the cytosolic membrane, followed by centrifugation and application of the supernatant containing the soluble His_6-tagged *Sl*Csp3 fusion protein to an immobilized nickel chromatography column.[1] Cleavage of the N-terminal His_6-tag from the *Sl*Csp3 protein is carried out using the serine protease, thrombin, followed by size-exclusion chromatography (Sephadex G75 resin). The *Sl*Csp3 elutes from the Sephadex G75 column at a retention volume consistent with a protein of mass corresponding to a homotetramer assembly.

MOLECULAR CHARACTERIZATION

The N-terminal sequence of recombinant *Sl*Csp3 retains three additional residues (Gly-Ser-His-Met*Sl*Csp3) before the Met1 following cleavage of the His_6-tag. On denaturing gel electrophoresis, a single Coomassie-stained band is observed that runs at a molecular weight corresponding to ~15 kDa. Under denaturing conditions, electrospray ionization mass spectrometry (ESI-MS) reports a mass for the recombinant *Sl*Csp3 of 14 604.6 Da, corroborating the presence of the N-terminal Gly-Ser-His sequence.[1] Application of *Sl*Csp3 to native ESI-MS leads to the identification of a dominant species with a mass of 58 418.16 Da, consistent with *Sl*Csp3 existing in solution as a homotetramer assembly, that is four protomers, consistent with the elution profile from size-exclusion chromatography.[1] Notably, the mass obtained from native ESI-MS is accountable for only the protein, and thus the recombinant *Sl*Csp3 does not purify with bound copper ions.[1]

SPECTROSCOPY OF SlCsp3

Addition of cupric ions to the as-purified *Sl*Csp3 results in no spectral changes in either the ultraviolet (UV) or visible regions of the electronic absorbance spectrum. To assess cuprous ion binding to *Sl*Csp3, strict anaerobic conditions are required, with stock Cu^{I} concentrations first determined spectrophotometrically through titration to a known concentration of the Cu^{I}-specific bidentate ligand, bicinchoninic acid (BCA) (Figure 1(a)). Formation of the $[Cu(BCA)_2]^{3-}$ complex gives an electronic absorbance spectrum with a λ_{max} at 562 nm and an extinction coefficient (ε) of 7900 M^{-1} cm^{-1} (Figure 1(b)),

This article was published in the *Encyclopedia of Inorganic and Bioinorganic Chemistry* in 2021 by John Wiley & Sons, Ltd.
DOI: 10.1002/9781119951438.eibc2777

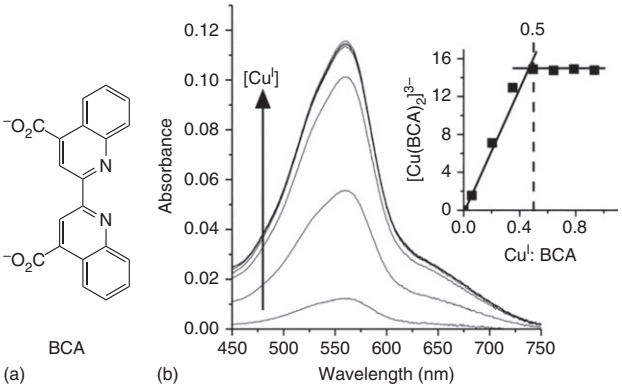

Figure 1 (a) Chemical structure of [2,2-biquinoline]-4,4′-dicarboxylic acid, commonly referred to as bicinchoninic acid (BCA). (b) Absorbance spectra obtained by titrating a CuCl solution into a known concentration of BCA. The absorbance increase at 562 nm is linear with a sharp turning point at a Cu^{I}:BCA of 0.5 (*inset*), indicating the formation of a 1:2 $[Cu(BCA)_2]^{3-}$ complex.

enabling for stock Cu^{I} concentrations to be determined upon saturation of the BCA ligand (Cu^{I}:BCA stoichiometry of 0.5, Figure 1(b) *inset*).[32] Titration of Cu^{I} to *Sl*Csp3 results in the gradual appearance in the UV region of the spectrum of (Cys)Sγ → Cu^{I} ligand-to-metal charge transfer (LMCT) bands (Figure 2(a)), which increase concomitantly with increasing [Cu^{I}] until a saturation point is reached coinciding with a stoichiometry of between 18 and 20 bound Cu^{I} ions per *Sl*Csp3 protomer (Figure 2(b)).[1] Thus, ~80 Cu^{I} ions can bind per *Sl*Csp3 homotetramer.

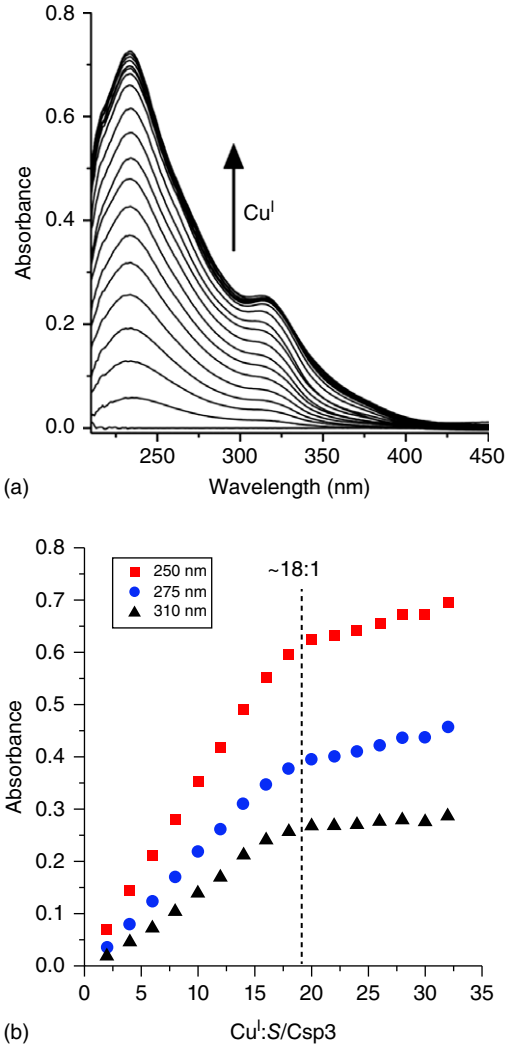

Figure 2 UV-absorbance spectroscopy and stoichiometry of Cu^{I} binding to *Sl*Csp3 at pH 7.5. (a) UV spectral changes for *Sl*Csp3 upon addition of increasing stoichiometries of cuprous ions. (b) Absorbance changes for selected wavelengths plotted as a function of the Cu^{I}:*Sl*Csp3 ratio. The dashed lines indicate a break point in the titration where the stoichiometry of Cu^{I} binding can be estimated.[1] [Straw, M. L., Chaplin, A. K., Hough, M. A., Paps, J., Bavro, V. N., Wilson, M. T., Worrall, J. A. R. (2018). A cytosolic copper storage protein provides a second level of copper tolerance in *Streptomyces lividans*. *Metallomics*, **10**(1), 180–193.]

X-RAY STRUCTURE OF *Sl*Csp3

Crystallization

Crystals of the apo and Cu^{I}-loaded forms of *Sl*Csp3 were grown from 1.4 M ammonium sulfate solutions buffered with either 0.1 M HEPES (2-[4-(2-hydroxyethyl)piperazin-1-yl]ethanesulfonic acid), pH 7.0, for the apo form or 0.1 M MES (2-(*N*-morpholino)ethanesulfonic acid), pH 6.0, for the Cu^{I}-loaded form. Cu^{I}-loaded samples for crystallization were prepared by the addition of a 25-fold excess over apo protein concentration of Cu^{I} ions with unbound Cu^{I} removed using a desalting column.[1] Crystals of the apo protein had a hexagonal lattice and a $P6_122$ space group with a unit cell of $a = 93.6$ Å, $b = 93.6$ Å, and $c = 213.4$ Å (1 Å = 0.1 nm) that contained four protomers (i.e. 4 four-helix bundle motifs) in the asymmetric unit. In the case of the Cu^{I}-loaded protein, crystals had an orthorhombic lattice and an *I*222 space group with a unit cell of $a = 93.6$ Å, $b = 93.6$ Å, and $c = 213.4$ Å and one protomer in the asymmetric unit. The apo and Cu^{I}-loaded structures were determined using molecular replacement and refined to a resolution of 1.34 and 1.50 Å, respectively (Table 1).[1]

Structure of apo *Sl*Csp3

Each of the four protomers present in the crystallographic asymmetric unit of apo *Sl*Csp3 exclusively comprises four α-helices, which pack together lengthways in an antiparallel

This article was published in the *Encyclopedia of Inorganic and Bioinorganic Chemistry* in 2021 by John Wiley & Sons, Ltd.
DOI: 10.1002/9781119951438.eibc2777

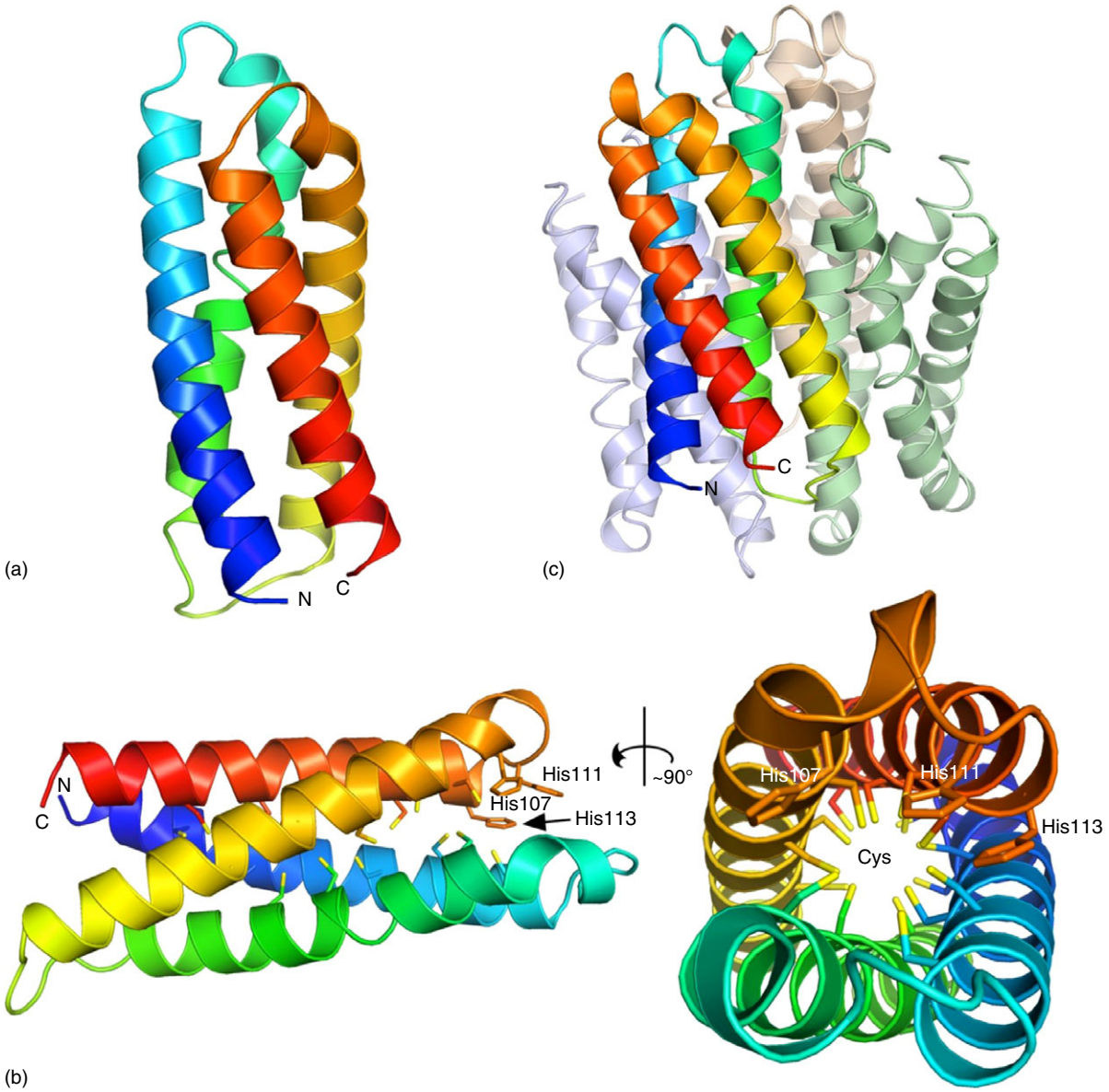

Figure 3 Cartoon representation of the X-ray structure of apo *Sl*Csp3 (PDB code: 6EI0).[1] (a) The up-down–up-down topology of the four-helix bundle (protomer) with the N and C termini labeled. (b) Side-on and core views of the four-helix bundle. The three His residues at the entrance to the core and the Cys residues lining the core are shown in stick representation. (c) The functional homotetramer assembly of *Sl*Csp3. [Based on ML Straw, AK Chaplin, MA Hough, J Paps, VN Bavro, MT Wilson, E Vijgenboom, JAR Worrall, *Metallomics*, **10**, 180–193 (2018).]

manner to give a four-helix bundle motif with an up-down–up-down topology (Figure 3(a)).[1] The dimensions of the four-helix bundle are ~29 × 47 × 38 Å. The 18 Cys residues present in *Sl*Csp3 face inward into the solvent-excluded core of the bundle (Figure 3(b)).[1] Notably, Csp3s have a higher proportion of Cys residues compared to Csp1s, suggesting a higher Cu^{I} storage capacity.[1,4,33] No disulfide bonds or chemical modifications to any of the Cys residues were observed in the crystal structure, and thus all Cys thiolates are free to coordinate a Cu^{I} ion. At one end of the four-helix bundle, access to the Cys core is via an opening lined with hydrophilic residues, dominated by a triad of His residues (Figure 3(b)), which are highly conserved across Csp3 members.[1,4,33] At the opposite end of the His triad, a stretch of hydrophobic side chains must be navigated before access to the Cys core is reached, and thus the His entrance is favored for Cu^{I} ion entry (*vide infra*).

In solution, the functional structure of *Sl*Csp3 is a homotetramer (Figure 3(c)), with the dimensions of ~55 × 61 × 55 Å. The total solvent-accessible surface area of the homotetramer assembly is 17 320 $Å^2$, with a buried area, defined as the total solvent-accessible surface

This article was published in the *Encyclopedia of Inorganic and Bioinorganic Chemistry* in 2021 by John Wiley & Sons, Ltd.
DOI: 10.1002/9781119951438.eibc2777

area buried upon formation of all assembly interface, of 8105 Å^2.[34] Thus, nearly 50% of the total accessible solvent surface area of the tetramer is part of the interface between protomers. This is reflected in the following thermodynamic parameters: the solvation free energy gain upon formation of the assembly, $\Delta G^{Int} = -53.2\,kcal\,mol^{-1}$ and the free energy of assembly dissociation, $\Delta G^{diss} = 24.4\,kcal\,mol^{-1}$, where the large negative ΔG^{Int} value and a $\Delta G^{diss} \gg 0$ implies a highly thermodynamically stable functional assembly.[34]

Coordination chemistries of the Cu^I-loaded *Sl*Csp3

The positions of the cuprous ions in the X-ray structure of the Cu^I-loaded *Sl*Csp3 were identified from anomalous difference maps.[1] These revealed well-defined electron density

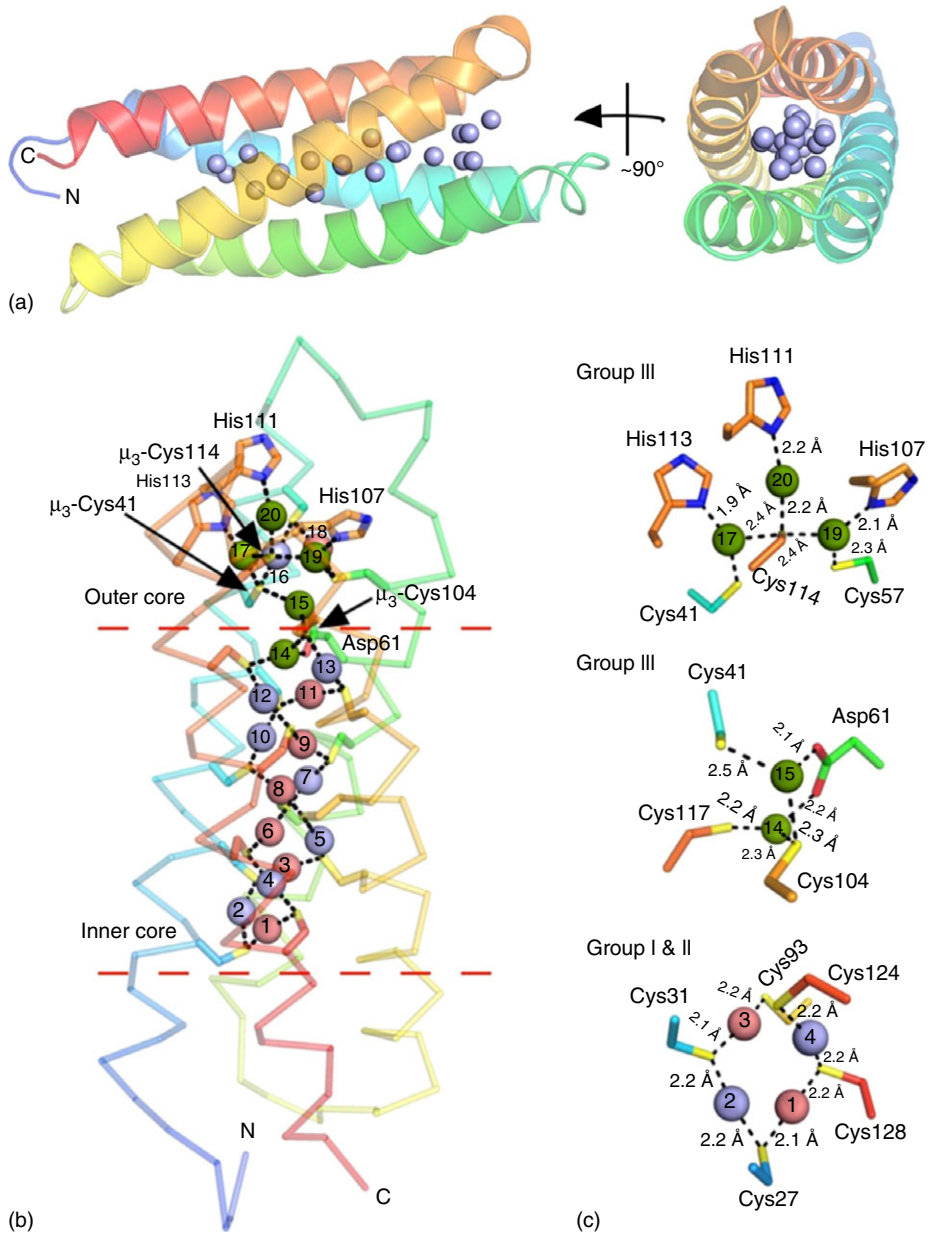

Figure 4 The X-ray structure of Cu^I-loaded *Sl*Csp3 (PDB code: 6EK9).[1] (a) Spatial positions of the 20 cuprous ions (spheres) bound in a protomer. (b) An overall view of the coordination chemistry of the bound Cu^I ions in the outer and inner cores of a protomer. The Cu^I ions (spheres) are color coded according to their coordination group classification: group I, blue; group II, pink; group III, green. The Cys residues that participate in μ_3-S-Cys coordination chemistry are labeled. (c) Specific examples of coordination chemistry among the different groups, with bond distances between the Cu^I ions and respective ligand indicated. [Based on ML Straw, AK Chaplin, MA Hough, J Paps, VN Bavro, MT Wilson, E Vijgenboom, JAR Worrall, *Metallomics*, **10**, 180–193 (2018).]

This article was published in the *Encyclopedia of Inorganic and Bioinorganic Chemistry* in 2021 by John Wiley & Sons, Ltd.
DOI: 10.1002/9781119951438.eibc2777

Table 2 The cuprous ions in *Sl*Csp3 that participate in the three classified coordination groups and the 15 copper ions that make up the nine Cu(I)–Cu(I) interactions

Coordination group	Cu^I number	Cu^I–Cu^I interaction	Distance (Å)
Group I	Cu2, Cu4, Cu5, Cu7, Cu10, Cu12, Cu13, Cu16	Cu1–Cu2	2.8
Group II	Cu1, Cu3, Cu6, Cu8, Cu9, Cu11, Cu18	Cu4–Cu6	2.6
Group III	Cu14, Cu15, Cu17, Cu19, Cu20	Cu7–Cu8	2.8
		Cu9–Cu10	2.8
		Cu13–Cu14	2.7
		Cu14–Cu15	2.8
		Cu16–Cu17	2.5
		Cu16–Cu18	2.7
		Cu18–Cu19	2.6

[Based on ML Straw, AK Chaplin, MA Hough, J Paps, VN Bavro, MT Wilson, E Vijgenboom, JAR Worrall, *Metallomics*, **10**, 180–193 (2018).]

for 20 cuprous ions filling the core of the four-helix bundle,[1] thus confirming earlier titration data (Figure 2(b)) and implying that the functional homotetramer has the capacity to bind a total of 80 cuprous ions. Csps are the only example in biology where the four-helix bundle fold is utilized to be completely filled with metal ions. Other examples of metalloproteins and enzymes that utilize a four-helix bundle fold are ferritins (see ***Ferritin***)[35] and sMMO (see ***Methane Monooxygenase Hydroxylase***),[12] both of which house a diiron center and cytochrome b_{562} (see ***b-Type Cytochrome Electron Carriers: Cytochromes b_{562} and b_5, and Flavocytochrome b_2***),[36] which houses a single heme group. The spatial positions of the 20 Cu^I ions in the core are shown in Figure 4(a) and have been divided into either the inner (Cu sites 1–14) or the outer (Cu sites 15–20) cores (Figure 4(b)).[1] All Cys residues coordinate the cuprous ions via the Sγ atom, with the Oδ and Nδ1 atoms from an Asp and three His residues, respectively, also contributing to the coordination sphere of several Cu^I ions (Figure 4(b)). Within the two cores, cuprous ion coordination has been grouped based on differences in the coordination environment of the Cu^I ion (Figure 4(c)). In group I, Cu^I ions are coordinated by two Cys thiolates in a CXXXC motif on the same helix. In group II, by two Cys thiolates on different helices of the four-helix bundle, and in group III, by Cys thiolates and either Asp or His residues (Figure 4(c)).[1] The Cu^I ions assigned to each coordination group are reported in Table 2.[1] At sites 1–13, the coordinating Cys residues bridge between two Cu^I ions (μ_2-S-Cys) with bond lengths varying between 2.0 and 2.3 Å (Figure 4(b) and (c)). The group III Cu14 and Cu15 ions have a three-coordinate trigonal geometry arising from two Cys residues and the carboxylate Oδ atoms of Asp61 (Figure 4(c)). In other Csp3 members, the Asp can be replaced by an Asn, but O coordination is still possible.[4] Cu17 and Cu19 (group III) also have three-coordinate trigonal geometries, with the third ligand derived from the Nδ1 atom of His113 and His107, respectively (Figure 4(c)). The third His in the triad, His111, also participates in Cu^I coordination to Cu20 (group III); however, this cuprous ion is not trigonally coordinated and is the only Cu^I ion not to have bis-Cys coordination (Figure 4(c)).[1] Instead, Cu20 adopts a near linear geometry with thiolate coordination from Cys114 (Figure 4(c)). Finally, three of the 18 Cys residues in *Sl*Csp3, Cys41, Cys104, and Cys114, each bridge three cuprous ions (μ_3-S-Cys); μ_3-S-Cys^{37}–Cu15-16-17; μ_3-S-Cys^{104}–Cu13-14-15; μ_3-S-Cys^{114}–Cu17-19-20 (Figure 4(b) and (c)).

A Cu^I to Cu^I distance of ≤2.8 Å can be considered to have some metal–metal bonding character as the van der Waals radius of copper is 1.4 Å. In *Sl*Csp3, 15 out of the 20 coordinated cuprous ions have Cu^I–Cu^I distances between 2.5 and 2.8 Å (Table 2), resulting in a total of nine Cu^I–Cu^I interactions (Table 2).[1]

FUNCTIONAL ASPECTS

Determination of an apparent Cu^I-binding constant for *Sl*Csp3

An estimation of apparent Cu^I-binding affinities in cuproproteins is most accurately determined through competition experiments using high-affinity chromogenic Cu^I bidentate ligands such as BCA (Figure 1(a)) under strict anaerobic conditions.[38] The formation of the $[Cu(BCA)_2]^{3-}$ complex has reported an overall formation constant (β_2) of log 17.7, which is essentially pH independent at pH ≥ 7.0.[39] To obtain an apparent Cu^I-binding affinity for *Sl*Csp3, a series of titration experiments were undertaken where the protein and BCA concentration remained fixed, but the $[Cu^I]$ varied.[1] At BCA concentrations of 50 and 100 μM, *Sl*Csp3 outcompeted the BCA ligand for Cu^I until >15 Cu^I equivalents, with respect to protein, were added (Figure 5(a) and *inset*).[1] Upon increasing the BCA concentration (250–1000 μM), competition for cuprous ions between *Sl*Csp3 and the BCA ligand was observed, leading to an estimation of maximum Cu^I occupancy

This article was published in the *Encyclopedia of Inorganic and Bioinorganic Chemistry* in 2021 by John Wiley & Sons, Ltd.
DOI: 10.1002/9781119951438.eibc2777

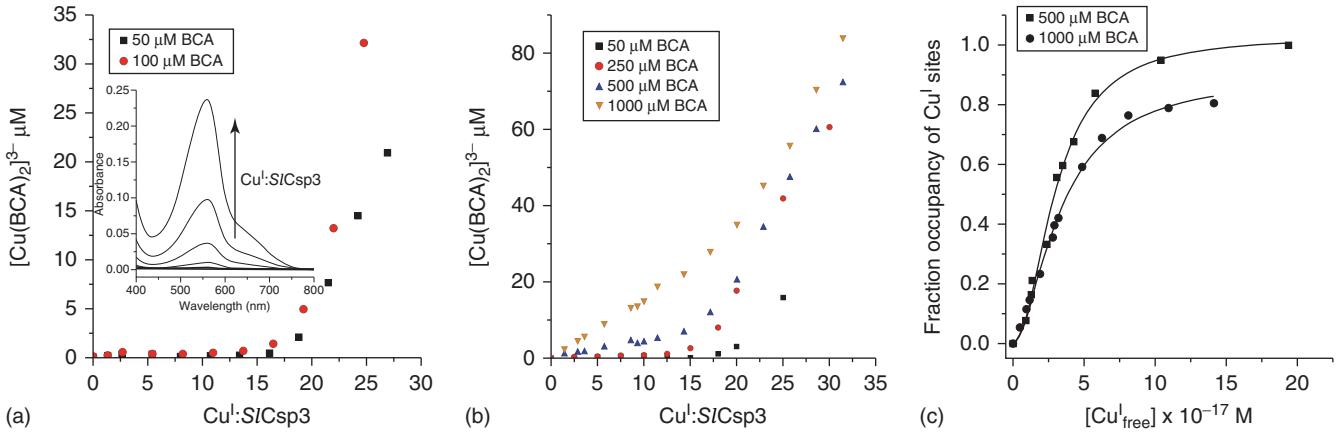

Figure 5 Determining the apparent Cu^I-binding affinity (K_{Cu}) of *Sl*Csp3 at pH 7.5. (a) Plot of $[Cu(BCA)_2]^{3-}$ versus the Cu^I:*Sl*Csp3 concentration generated from titrating Cu^I ions into *Sl*Csp3 in the presence of 50 and 100 μM BCA. The $[Cu(BCA)_2]^{3-}$ complex forms after the addition of 15 Cu^I equivalents. *Inset*, absorbance spectra indicating the formation of the $[Cu(BCA)_2]^{3-}$ complex upon addition of Cu^I to 5 μM *Sl*Csp3 in the presence of 100 μM BCA. (b) As in (a) but with a wider range (50–1000 μM) of BCA concentrations, illustrating that as the [BCA] increases beyond 250 μM, competition with *Sl*Csp3 for Cu^I ions occurs. (c) Determination of K_{Cu} for *Sl*Csp3 from plotting the fractional occupancy of Cu^I-binding sites in *Sl*Csp3 at varying $[Cu^I_{free}]$ determined from the plots at 500 and 1000 μM BCA in (b) using Equation 2. Data points have been fitted to the Hill equation.[1] [Based on ML Straw, AK Chaplin, MA Hough, J Paps, VN Bavro, MT Wilson, E Vijgenboom, JAR Worrall, *Metallomics*, **10**, 180–193 (2018).]

of ~15 Cu^I ions per *Sl*Csp3 protomer (Figure 5(b)).[1] Under these experimental conditions, an apparent Cu^I-binding affinity was determined using two approaches, both of which assume that the following two equilibria are present:

$$2BCA + Cu^I_f \rightleftharpoons Cu(BCA)_2 = K_{BCA}$$
$$S_f + Cu^I_f \rightleftharpoons Cu^IS = K_{Cu}$$

where BCA is the free ligand, S_f are the sites on *Sl*Csp3 that are unoccupied with Cu^I, Cu^I_f is free cuprous ions, and K_{BCA} and K_{Cu} are equilibrium dissociation constants for the affinities of Cu^I for BCA and *Sl*Csp3, respectively. Based on the above equilibria, the $[Cu^I_f]$ is given by

$$[Cu^I_f] = \frac{K_{BCA}[Cu(BCA)_2]}{[BCA]^2} = \frac{K_{Cu}[Cu^IS]}{[S_f]}$$

which can be rearranged to solve for K_{Cu}

$$K_{Cu} = \frac{K_{BCA}\left[Cu(BCA)_2\right]\left(\left[S_t\right] - \left[Cu^I_t\right] + \left[Cu\,(BCA)_2\right]\right)}{\left(\left[BCA_t\right] - 2\left[Cu(BCA)_2\right]\right)^2\left(\left[Cu^I_t\right] - \left[Cu(BCA)_2\right]\right)} \quad (1)$$

where $[S_t]$ is the total concentration of sites occupied in *Sl*Csp3, $[Cu^I_t]$ is the total concentration of cuprous ions added, and $[BCA_t]$ is the total concentration of the BCA ligand in the experiment. Using Equation 1 together with the data reported in Figure 5(b) (250–1000 μM BCA), an average K_{Cu} for *Sl*Csp3 of $3.3 \pm 1.3 \times 10^{-17}$ M has been reported.[1] Alternatively, at BCA concentrations ≥250 μM, the K_{Cu} can be determined by calculating the $[Cu^I_f]$ using Equation 2,

$$[Cu^I_f] = \frac{[Cu(BCA)_2]}{[BCA^*]^2\beta_2} \quad (2)$$

where $[BCA^*] = [BCA_t] - 2[Cu(BCA)_2]$, and β_2 is $\log 17.7$.[39] Plots of $[Cu^I_f]$ against the fractional Cu^I occupancy of *Sl*Csp3 at a given [BCA] display a sigmodal dependence, which given that the system is at equilibrium implies cooperativity of Cu^I binding (Figure 5(c)).[1] Using a nonlinear form of the Hill equation, an average K_{Cu} for BCA concentrations ranging between 250 and 1000 μM of $2.9 \pm 0.2 \times 10^{-17}$ M has been reported together with an average Hill coefficient, $n = 1.9 \pm 0.2$.[1]

The K_{Cu} determined for *Sl*Csp3 is consistent with the subfemtomolar values reported for *Bs*Csp3 and *Mt*Csp3,[4] demonstrating that the Cys-lined core of the four-helix bundle is a highly thermodynamically stable scaffold to retain Cu^I in the reducing environment of the bacterial cytosol. Notably, *Sl*Csp3 is the only Csp3 member so far studied for which cooperativity of Cu^I binding has been reported.[1] Cooperativity of cuprous ion binding has been reported for Csp1a, which binds 13 cuprous ions per four-helix bundle.[2] However, a note a of caution proceeds these observations, given that the $[Cu^I_f]$, which are exceedingly low, are calculated indirectly from binding to BCA.[1]

This article was published in the *Encyclopedia of Inorganic and Bioinorganic Chemistry* in 2021 by John Wiley & Sons, Ltd.
DOI: 10.1002/9781119951438.eibc2777

The effect of *Sl*Csp3 on the copper-dependent morphological development of *S. lividans*

Streptomycetes undergo a complex development lifecycle on solid substrates such as agar. Following spore germination, a vegetative mycelium is established that through branching results in a large network of hyphae.[40,41] In response to nutrient depletion and other signals, the initiation of both secondary metabolite production (e.g. compounds that have been found to possess antibiotic, antifungal, and anthelmintic properties) and morphological differentiation occurs.[37,42] The erection of an aerial mycelium takes place in this next phase, followed by differentiation, which leads to the production of millions of readily dispersible spores.[40,41] In *S. lividans*,[43] the bioavailability of copper ions has a strong influence on initiating the morphological switch from the vegetative to the aerial growth phase that coincides with the production of secondary metabolites.[44–50]

Under copper-limiting conditions, two extracytoplasmic copper metallochaperone proteins have been identified, Sco (synthesis of cytochrome c oxidase) and ECuC (extracytoplasmic copper chaperone), that together operate to facilitate delivery of copper to cytochrome c oxidase (CcO) and a novel mononuclear copper-radical oxidase, GlxA (galactose oxidase-like).[47–50] The enzymatic action of GlxA has been reported to be a key requirement to initiate the copper-dependent morphological development switch between vegetative and aerial hyphae.[49,50] Under copper stress, toxicity in the cytoplasm is precluded through the action of a Cu^{I}-sensing regulatory transcription factor,[51,52] which belongs to the copper sensitive operon regulator (CsoR) family.[53] Cuprous ions that accumulate in the cytosol are 'sensed' by the DNA-bound apo-CsoR, which has an apparent K_{Cu} of $\sim 10^{-18}$ M (attomolar) and may be considered as the cytosolic Cu^{I} 'set-point' concentration for triggering efflux.[51] The binding of Cu^{I} to the DNA-complexed apo-CsoR allosterically activates transcriptional derepression of three efflux systems, each comprising a P_1-type ATPase and a CopZ-like (copper resistance operon) Cu^{I} metallochaperone protein that act in synergy to rapidly efflux cuprous ions from the cytosol (see ***Copper Transporters and Chaperones***).[51,52,54] Thus, to balance the metabolic demands for morphological development and safeguard against Cu^{I} toxicity, *S. lividans* has evolved highly sophisticated metallostasis systems (processes that governs adaptive response to both metal restriction and metal overload) to maintain the cellular copper supply to essential cuproenzymes and protect the organism under copper stress.

To investigate the effect of *Sl*Csp3 on the copper-dependent morphological development and growth of *S. lividans*, a strain in which the *csp3* gene was deleted (Δ*csp3*) has been constructed.[1] On solid media (agar plates), growth and development of the Δ*csp3* strain at exogenous copper concentrations up to 200 μM were identical to that of the wild-type (WT) strain (Figure 6(a)).[1] However, at exogenous copper concentrations >200 μM, a clear phenotype for the Δ*csp3* strain was observed in

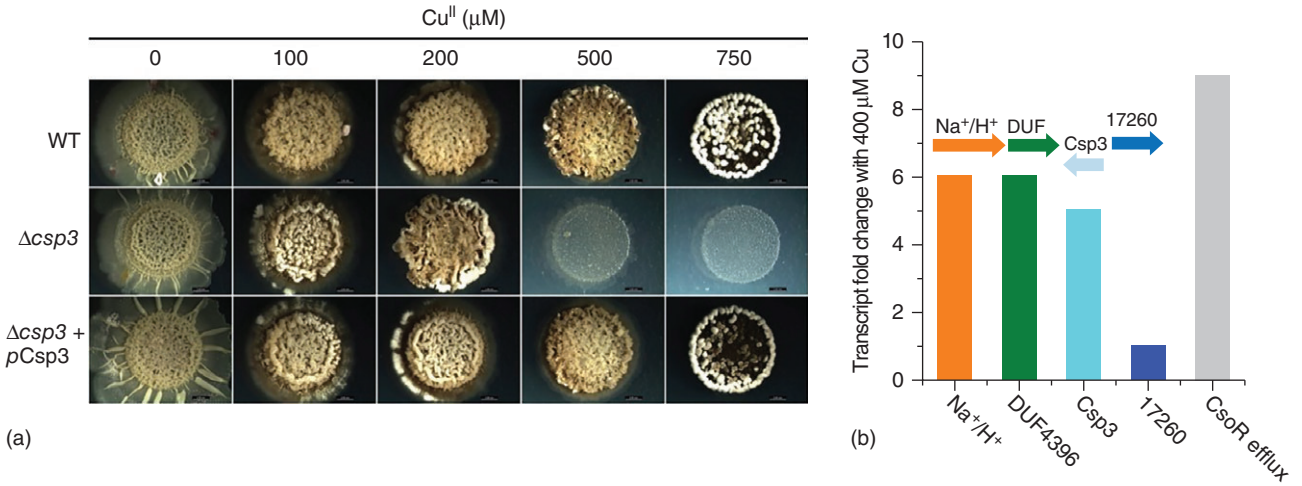

Figure 6 Functional aspects of *Sl*Csp3 *in vivo*. (a) Growth and development of the WT strain, the Δ*csp3* mutant strain, and the Δ*csp3* mutant strain complemented with the pCsp3 plasmid on defined agar media with glucose as the sole carbon source after six days growth at 30 °C in the presence of exogenous copper.[1] [Straw, M. L., Chaplin, A. K., Hough, M. A., Paps, J., Bavro, V. N., Wilson, M. T., … Worrall, J. A. R. (2018). A cytosolic copper storage protein provides a second level of copper tolerance in *Streptomyces lividans*. *Metallomics*, **10**(1), 180–193. doi:10.1039/c7mt00299h.] All images are of the same magnification. (b) Representation of the genomic environment (*inset*) and transcript fold increases determined from RNA-seq analysis of *csp3* and the adjacent genes in a liquid-grown *S. lividans* culture in the presence of 400 μM copper.[51] [Based on Dwarakanath, S.; Chaplin, A. K.; Hough, M. A.; Rigali, S.; Vijgenboom, E.; Worrall, J. A. R. (2012). Response to Copper Stress in *Streptomyces lividans* Extends beyond Genes under Direct Control of a Copper-sensitive Operon Repressor Protein (CsoR). *Journal of Biological Chemistry*, **287**(21), 17833–17847.]

This article was published in the *Encyclopedia of Inorganic and Bioinorganic Chemistry* in 2021 by John Wiley & Sons, Ltd.
DOI: 10.1002/9781119951438.eibc2777

which the development of aerial mycelium and spores is reduced or absent (Figure 6(a)).[1] Introduction of the *csp3* gene on a plasmid under transcriptional control of its own promoter to the Δ*csp3* strain leads to a reversal of the phenotype (Figure 6(a)).[1] Thus, *Sl*Csp3 is clearly required for growth and development of *S. lividans* at high copper concentrations (between 200 and 500 μM external copper, depending on the media used),[1] but at basal copper levels, the Δ*csp3* strain mirrors the growth of the parent strain.[1] To assess whether *Sl*Csp3 influences downstream copper-trafficking pathways in the extracytoplasmic environment under homeostasis, CcO activity was monitored in the Δ*csp3* strain.[1] No discernable differences in CcO activity for the Δ*csp3* strain compared to the parent strain were observed.[1] Under the experimental conditions employed, this observation precludes a downstream role (metabolic) for *Sl*Csp3 in supplying stored Cu^I to the extracytoplasmic environment to be utilized by the copper metallochaperones, Sco and ECuC, for metalation of CcO and GlxA.[1] In conclusion, the growth studies conducted to date are consistent with a role of *Sl*Csp3 in providing an increased level of copper tolerance in *S. lividans* and not as a store for metabolic purposes.[1]

Gene environment and transcriptional response under copper stress

The genomic environment of *Sl*Csp3 (Figure 6(b), *inset*) reveals two upstream genes predicted to encode for an Na^+/H^+ antiporter (SLI_RS17245) and a protein of 181 amino acids (SLI_RS17250) that belongs to the DUF4396 superfamily. Immediately downstream from *Sl*Csp3 is a gene annotated to encode for a precorrin-8x methyl mutase (SLI_RS17260). Changes in the transcriptome of *S. lividans* grown under copper stress have been investigated.[51] Transcript analysis was carried out by ribonucleic acid (RNA)-seq using liquid-defined cultures grown under homeostasis (i.e. basal copper conditions) and in the presence of 400 μM copper, with the data revealing an extensive array of up- and downregulated transcripts in response to growth under heightened copper levels.[51] As expected, genes under the control of the CsoR were significantly upregulated.[51] Transcript levels for the Na^+/H^+ antiporter, DUF4396, and *Sl*Csp3 also increased ~fivefold, but SLI_RS17260 was unaffected (Figure 6(b)). Notably, the copper-induced expression of the *Sl*Csp3 cluster was at a similar level to that observed for the efflux systems regulated by CsoR (Figure 6(b)). Regulation of *Sl*Csp3 is not under the control of the CsoR, as demonstrated through a lack of a recognizable consensus CsoR-binding site in the *Sl*Csp3 promoter region[1] and from the induction of expression in a Δ*csoR* strain of *S. lividans*.[51] Together with the observations from the growth assays, the RNA-seq data would suggest that once the CsoR/CopZ/P_1-type ATPase efflux systems become saturated, a second layer of copper-responsive transcription is operating on top of the CsoR regulon, which expresses *Sl*Csp3, the Na^+/H^+ antiporter, and DUF4396, enabling organism growth at higher copper levels.[1]

A copper metallochaperone can load Cu^I ions to apo-*Sl*Csp3

If the function of *Sl*Csp3 is to assist in copper tolerance and help sequester cuprous ions when the CsoR-regulated efflux systems become saturated, then it can be assumed that *Sl*Csp3 obtains its copper in a controlled manner such as through interaction with either a low-molecular-weight ligand (LMWL), for example mycothiol, the dominant thiol in Actinobacteria that is equivalent to glutathione in other bacteria,[55] or by a designated protein. Metal trafficking from a donor to an acceptor has been shown *in vitro* to occur through transient interactions that initiate a ligand-exchange mechanism to facilitate the transfer of the metal (i.e. the metal is never dissociated into solution).[56] Trafficking of Cu^I in the cytosol of *S. lividans* under homeostasis and stress has been reported to involve CopZ-like Cu^I metallochaperones.[51,52] Using a size-exclusion chromatography-based approach, Cu^I-loaded CopZ has been shown to transfer copper to *Sl*Csp3, but Cu^I-loaded *Sl*Csp3 cannot transfer Cu^I to CopZ, at least under the stoichiometric conditions employed.[1] Thus, the ability of CopZ to safely 'off-load' its copper cargo fits with the view obtained from *in vivo* and transcriptional studies that the *Sl*Csp3 can assist in increasing the copper tolerance levels of *S. lividans*.

FUNCTIONAL DERIVATIVES

Understanding the kinetic and thermodynamic intricacies associated with Cu^I loading to *Sl*Csp3 is particularly challenging, considering the number of distinct binding sites that Cu^I thiolate chemistry can allow. The *in vitro* mechanism of cuprous ion loading to *Sl*Csp3 has been investigated using X-ray crystallography, stopped-flow kinetics, and site-directed mutagenesis.[57]

Visualization of Cu^I loading to *Sl*Csp3 through X-ray crystallography

X-ray crystal structures of *Sl*Csp3 have been determined following the addition of substoichiometric equivalents (5- and 10- equivalents) of cuprous ions.[57] For 5- equivalents, anomalous electron density associated with bound cuprous ions was only observed in the outer core (Figure 7(a)), revealing two types of multinuclear copper clusters.[57] Both clusters are dominated by group II and III coordination

This article was published in the *Encyclopedia of Inorganic and Bioinorganic Chemistry* in 2021 by John Wiley & Sons, Ltd.
DOI: 10.1002/9781119951438.eibc2777

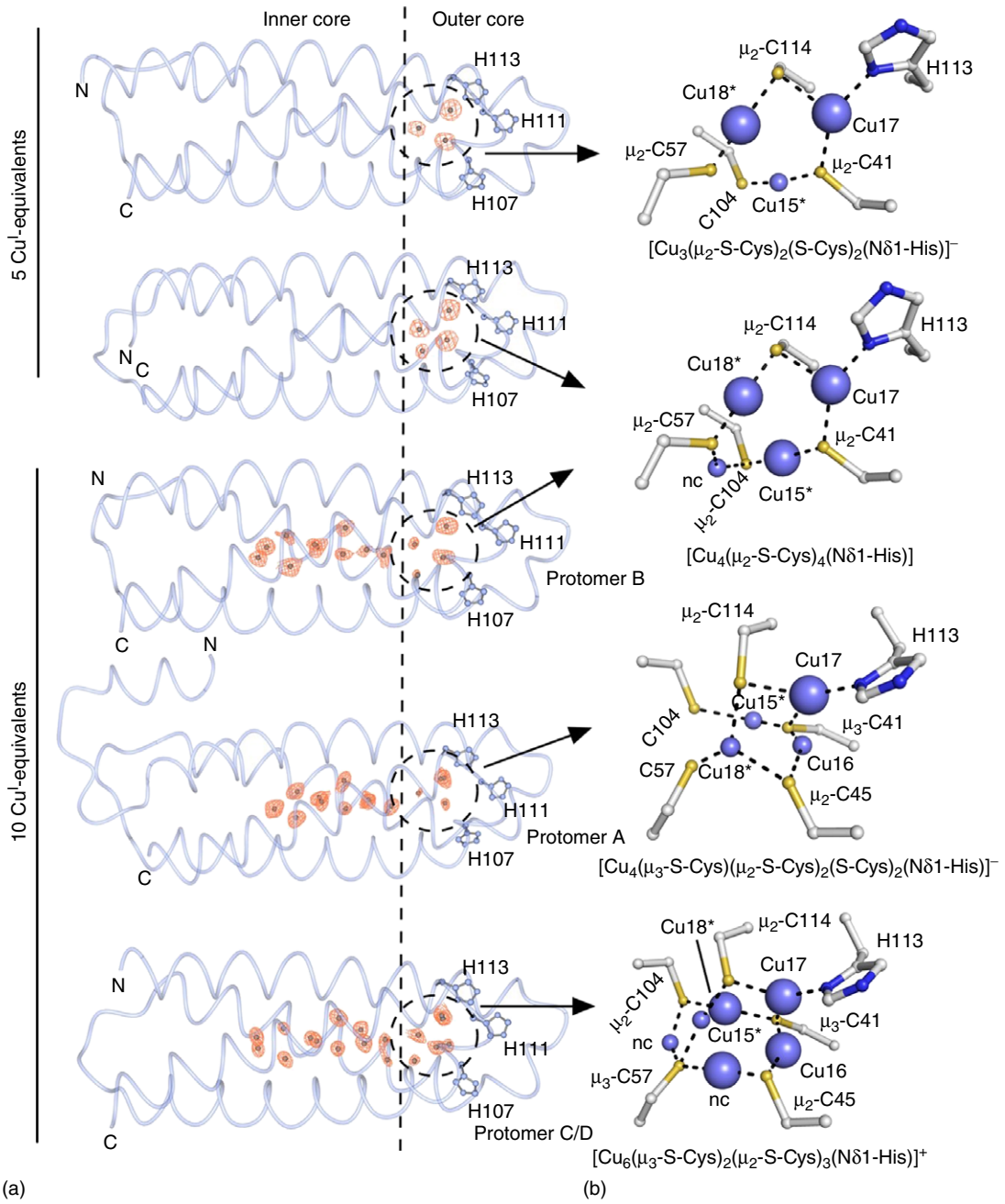

Figure 7 Visualization of Cu^{I} sites and polynuclear Cu^{I} clusters upon partial Cu^{I} loading of *Sl*Csp3. (a) X-ray structures indicating the distribution of the coordinated Cu^{I} ions (silver spheres) following addition of 5 or 10 Cu^{I} equivalents. Worm representation of individual protomers found in the respective crystallographic asymmetric unit following addition of 5 or 10 Cu^{I} equivalents, with the anomalous electron density (orange mesh) revealing the location of coordinated cuprous ions. The His residues at the outer core entrance are depicted in sticks and labeled. (b) Ball-and-stick representation of the various polynuclear Cu^{I} clusters identified in the outer core of the protomers (dashed circle in (a)). [Straw, Megan L., Hough, Michael A., Wilson, Michael T., Worrall, Jonathan A.R. (2019). A histidine residue and a tetranuclear cuprous-thiolate cluster dominate the copper loading landscape of a copper storage protein from *Streptomyces lividans*. *Chemistry – A European Journal*, **25**, 10678–10688.]

chemistry, creating a negatively charged trinuclear $[Cu_3(\mu_2\text{-S-Cys})_2(\text{S-Cys})_2(N\delta1\text{-His})]^-$ cluster (observed in one protomer of the crystallographic asymmetric unit) and a neutral, tetranuclear $[Cu_4(\mu_2\text{-S-Cys})_4(N\delta1\text{-His})]$ cluster (observed in three of the protomers in the crystallographic asymmetric unit) (Figure 7(a) and (b)).[57] The latter is symmetrical in that all Cys thiolates are bridging (μ_2-S-Cys) a Cu^{I} ion, whereas in the trinuclear cluster, the symmetry

This article was published in the *Encyclopedia of Inorganic and Bioinorganic Chemistry* in 2021 by John Wiley & Sons, Ltd.
DOI: 10.1002/9781119951438.eibc2777

is broken as two Cys thiolates display monodentate Cu^{I} coordination (Figure 7(b)). In both clusters, only one cuprous ion occupies a binding site observed in the fully Cu^{I}-loaded protein (Cu17).[57] Two cuprous ions, although occupying similar positional locations to Cu15 and Cu18 in the fully Cu^{I}-loaded structure, are distinct in that they have an altered coordination sphere and have been designated Cu15* and Cu18*.[57] The fourth cuprous ion in the tetranuclear cluster is coordinated at a site which is absent in the fully Cu^{I}-loaded protein and has been designated as a noncognate site and possesses group II coordination (Figure 7(b)).[57] In the trinuclear cluster, Cu15* has a lower occupancy than either Cu17 or Cu18*, while in the tetranuclear cluster, the noncognate copper has the lowest occupancy,[57] suggesting that the trinuclear cluster is an intermediate on route to forming the tetranuclear cluster.[57] Furthermore, sites 1–14 in the inner core remain unoccupied and suggest that the tetranuclear $[Cu_4(\mu_2\text{-S-Cys})_4(N\delta1\text{-His})]$ cluster must be thermodynamically more favored than occupancy of sites in the inner core, at least under low Cu^{I} ratios.[57]

The 10 Cu^{I}-equivalents structure reveals more sites occupied than Cu^{I} equivalents added, indicating that some of the sites are not fully occupied (Figure 7(a)).[57] Of the four protomers present in the crystallographic asymmetric unit, protomers A and B revealed electron density for 14 cuprous ions, with protomer A having all cuprous ions occupying cognate sites, while protomer B possesses two cuprous ions occupying noncognate sites.[57] In protomers C and D, anomalous electron density was observed for 18 cuprous ions. Copper sites 1, 2, and 4, located at the bottom of the inner core, remain unoccupied in all protomers, as do Cu sites 19 and 20.[57] The observation of different distributions and occupancies of cuprous ions within the inner and outer cores of *Sl*Csp3 reflect transient intermediates in the site occupancies during the Cu^{I}-loading process.[57] Notably, the polynuclear copper clusters identified in the outer core of the 5-equivalent structure also dominate in the 10-equivalents structure (Figure 7(b)).[57] In protomer B, the neutral symmetrical tetranuclear copper cluster is present (Figure 7(b)). However, in protomer A, a new asymmetric negatively charged tetranuclear $[Cu_4(\mu_3\text{-S-Cys})(\mu_2\text{-S-Cys})_2(\text{S-Cys})_2(N\delta1\text{-His})]^-$ cluster is observed (Figure 7(b)), whereas in protomers C and D, the tetranuclear clusters observed in protomers A and B combine with a second noncognate cuprous ion to form a positively charged hexanuclear $[Cu_6(\mu_3\text{-S-Cys})_2(\mu_2\text{-S-Cys})_3(N\delta1\text{-His})]^+$ cluster (Figure 7(b)). Thus, as more Cu^{I} ions are loaded to *Sl*Csp3, the outer core displays coordination promiscuity, enabling the formation of various polynuclear clusters, which are not observed in the inner core.

Stopped-flow kinetics to monitor Cu^{I} loading to *Sl*Csp3

Stopped-flow absorption spectroscopy has demonstrated that complete loading of aqueous Cu^{I} to *Sl*Csp3 is accomplished within the first 2 s of the reaction time course (Figure 8(a)).[57] For complete loading to occur within 2 s,

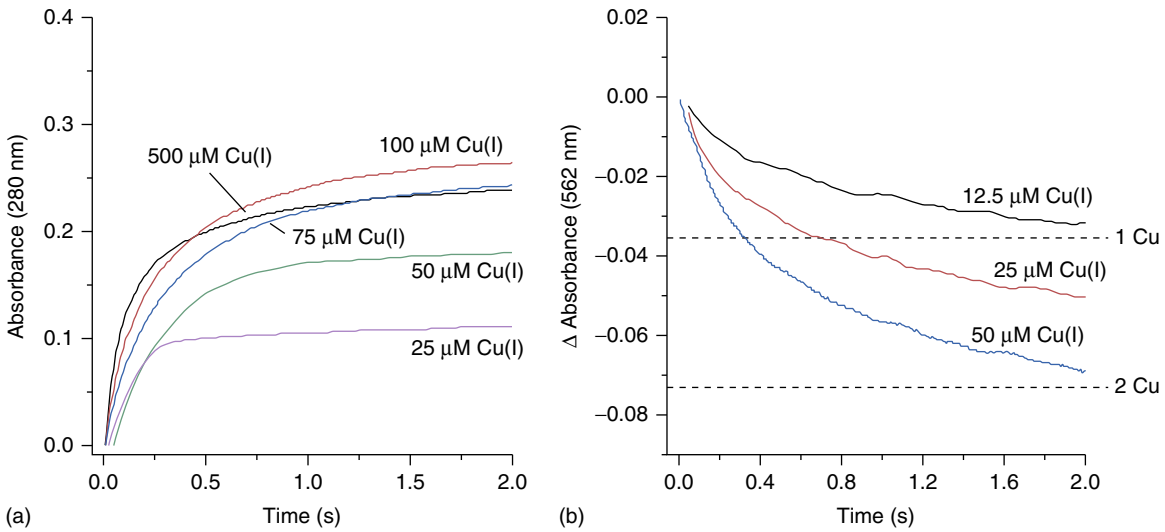

Figure 8 Kinetic time courses upon mixing various concentrations of aqueous Cu^{I} (a) and the $[Cu(BCA)_2]^{3-}$ complex (b) with *Sl*Csp3 in a stopped-flow spectrophotometer. In both the cases, the initial fast phase over the first 2 s of the reaction is depicted. In (b), the dashed lines indicate the expected absorbance changes for removal of Cu^{I} equivalents from the $[Cu(BCA)_2]^{3-}$ complex. Experiments were carried out at 20 °C at pH 7.5.[57] [Straw, Megan L., Hough, Michael A., Wilson, Michael T., Worrall, Jonathan A.R. (2019). A histidine residue and a tetranuclear cuprous-thiolate cluster dominate the copper loading landscape of a copper storage protein from Streptomyces lividans. *Chemistry – A European Journal*, **25**, 10678–10688.]

This article was published in the *Encyclopedia of Inorganic and Bioinorganic Chemistry* in 2021 by John Wiley & Sons, Ltd.
DOI: 10.1002/9781119951438.eibc2777

the individual binding sites within the four-helix bundle, although having a high intrinsic affinity for cuprous ions, must be able to pass Cu^I ions between sites, suggesting that an internal ligand-exchange-type mechanism is operating.[57] Based on the kinetics of Cu^I loading, this would mean that the half-life for Cu^I dissociation from any site within the core of the four-helix bundle will be $\ll$2 s.[57]

The kinetics of Cu^I loading to *Sl*Csp3 from a donor, BCA, have also been investigated using stopped-flow.[57] These studies revealed a rapid decrease in absorbance of the 562 nm peak of the $[Cu(BCA)_2]^{3-}$ complex, within the first 2 s of the reaction, when mixing fixed concentrations of $[Cu(BCA)_2]^{3-}$ with *Sl*Csp3.[57] The amplitude of this absorbance change was found to be $[Cu(BCA)_2]^{3-}$ concentration dependent,[57] and depending on the $[Cu(BCA)_2]^{3-}$ concentration mixed, between 1 and 2 Cu^I ions were found to be loaded to *Sl*Csp3 within the 2-s time period (Figure 8(b)).[57] Notably, over a time base of 500 s, multiple kinetic processes comprising at least three exponential phases were observed.[57] Such complexity in the kinetics must arise from the cuprous ions being delivered from the $[Cu(BCA)_2]^{3-}$ complex one at a time and involve (i) complex formation between *Sl*Csp3 and $[Cu(BCA)_2]^{3-}$, (ii) Cu^I transfer, and (iii) dissociation of the free BCA ligand.[57] Thus, the kinetic data imply a sequential mechanism of Cu^I loading to *Sl*Csp3, which is initiated through the transfer of a cuprous ion from a donor to a first coordination site in *Sl*Csp3, followed by the passage of cuprous ions from site to site within the core of the four-helix bundle.[57]

The role of the outer core His residues in Cu^I loading

When *Sl*Csp3 is fully Cu^I loaded (20 cuprous ions), all three His residues at the entrance to the outer core participate in group III coordination (Figure 4(b)).[1] When partially loaded (5 or 10 Cu^I equivalents added), His113 coordinates a cuprous ion, whereas His107 and His111 do not, implying a role for His107 and His111 in initial Cu^I capture.[57] Using site-directed mutagenesis to create the H107A, H111A, H113A, and H107A/H111A variants, the role that these His residues play in Cu^I loading has been elucidated.[57] The X-ray crystal structures for the fully Cu^I loaded, H111A, H113A, and H107/H111A variants have been determined, with all three structures revealing electron-density for copper sites 1–14 (inner core) with identical coordination chemistry as found in the WT protein.[57] In the outer core, an additional non-cognate Cu^I ion is present in all three variants adjacent to Cu15 (Figure 9(a)), with coordination from the Oδ atom of Asp61 and the Sγ atom of Cys57, creating a new group III coordination site.[57] No electron density was visible for Cu19 and Cu20 in the H111A and H107A/H111A structures (Figure 9(a)), thus supporting a role for these residues in initial Cu^I loading and also indicating their requirement in enabling a maximum of 20 cuprous ions to bind per four-helix bundle.

Stopped-flow kinetic studies of Cu^I loading to the His variants using BCA as the Cu^I donor revealed rapid transfer (again within the first 2 s) of Cu^I from the $[Cu(BCA)_2]^{3-}$ complex to the H111A and H113A variants (Figure 9(b)).[57] In contrast, the H107A and H107A/H111A variants both demonstrated a pronounced decrease in the rate of Cu^I entry, implying that His107 has a major role in the initial loading of Cu^I to *Sl*Csp3 (Figure 9(b)).[57] Furthermore, the H107A variant was additionally found to slow subsequent Cu^I transfer (i.e. after initial loading), which was also the case for the H111A variant, whereas the double variant (H107A/H111A) affected both the initial Cu^I loading (His107) and subsequent transfer (His107 and His111).[57] Finally, the kinetics of the H113A variant were identical to the WT protein corroborating structural interpretation that His113 impairs neither the initial Cu^I binding nor subsequent transfer to other available sites.

A mechanism for Cu^I loading to *Sl*Csp3

Based on the available kinetic, structural, and site-directed mutagenesis data, a mechanistic model accounting for Cu^I loading to *Sl*Csp3 using the $[Cu(BCA)_2]^{3-}$ complex as Cu^I donor has been proposed.[57] The model describes the relative energy of binding to the Cu^I sites in *Sl*Csp3 and illustrates the relative stability of the complexes of Cu^I in the sites described (Figure 10).[57] On mixing the coordinatively saturated $[Cu(BCA)_2]^{3-}$ complex with *Sl*Csp3, a heteroleptic complex forms, consisting of $[Cu(BCA)]^-$ and a nitrogen from a His residue, with the net loss of a BCA ligand (Figure 10). The His residue involved in this heteroleptic complex is His107 based on the large effect its removal has on the kinetics of the initial fast phase of Cu^I loading.[57] Furthermore, the effect His107 has on the initial Cu^I loading can be accounted for by the requirement for a transient ($[Cu(BCA)]^-$:His-*Sl*Csp3) complex to form and then dissociate after each Cu^I ion is donated.[57] An energetically favored transfer to sites 19 and 20 then follows before moving on to sites 15^*, 17, and 18^* to form first, the trinuclear and then the more thermodynamically stable tetranuclear cluster (Figures 7(b) and 10). On doing so, His107 is released from coordination and enables further Cu^I capture from the donor (His-ligand cycle, Figure 10). Removing His107 and His111 revealed that the movement of Cu^I ions beyond sites 19 and 20 following the initial binding is slowed. This is accounted for by His107 and His111 acting to stabilize Cu^I binding to sites 19 and 20, which when absent destabilizes these sites and hinders subsequent loading, which must occur via sites 19 and 20, followed by transfer into the outer core.[57]

Under low Cu^I stoichiometries, the formation of the neutral $[Cu_4(\mu_2\text{-S-Cys})_4(N\delta1\text{-His})]$ cluster creates an unfavorable barrier to loading into the inner core. To load Cu^I

This article was published in the *Encyclopedia of Inorganic and Bioinorganic Chemistry* in 2021 by John Wiley & Sons, Ltd.
DOI: 10.1002/9781119951438.eibc2777

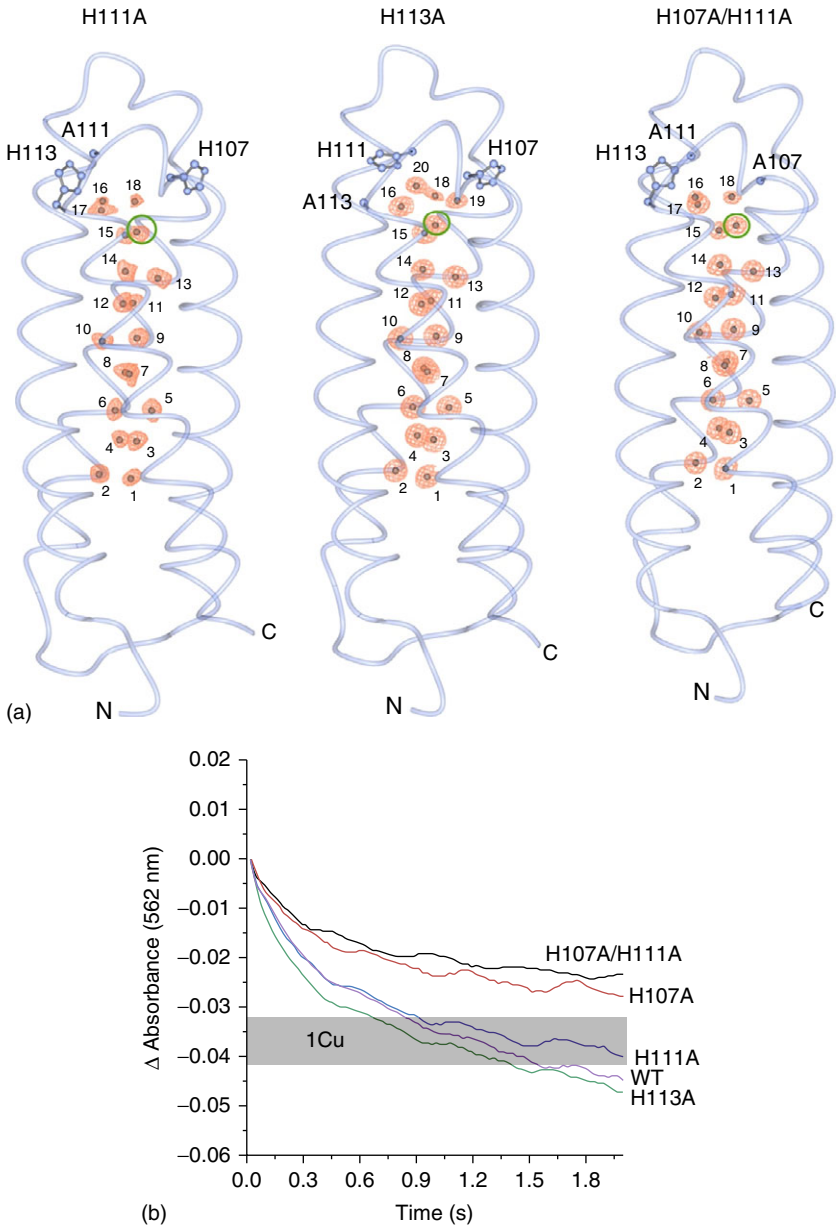

Figure 9 X-ray structures and stopped-flow absorbance kinetics of the *Sl*Csp3 His variants. (a) Worm representations of each His variant with the anomalous electron density for the bound Cu^{I} ions shown in orange mesh. The green circles indicate the location of the noncognate Cu^{I}-binding sites. (b) Reaction time course, illustrating the initial fast phase, on mixing the WT *Sl*Csp3 and each His variant with the $[Cu(BCA)_2]^{3-}$ complex (50 μM). Shaded area indicates the expected absorbance changes for removal of one Cu^{I} equivalent from the $[Cu(BCA)_2]^{3-}$ complex based on the variation of protein concentrations used in the experiment (20 °C, pH 7.5).[57] [Modified from Straw, Megan L., Hough, Michael A., Wilson, Michael T., Worrall, Jonathan A.R. (2019). A histidine residue and a tetranuclear cuprous-thiolate cluster dominate the copper loading landscape of a copper storage protein from Streptomyces lividans. *Chemistry – A European Journal*, **25**, 10678–10688.]

into the inner core via sites 14 and 15, interaction with the Oδ atoms of Asp61 must occur (Asp sites, Figure 10). A hard ligand/soft metal interaction is less favored and of lower affinity than the Cu^{I} thiolate coordination dominating the tetranuclear cluster. However, as more Cu^{I} is loaded into the outer core, this barrier is seemingly overcome, leading to transfer into the inner core becoming favorable. The visualization of Cu^{I} loading to *Mt*Csp3 has also been reported, with several X-ray structures determined following the addition of substoichiometric cuprous ions (Table 1).[33] Interestingly, for *Mt*Csp3, tetranuclear copper cluster formation $[Cu_4(\mu_2\text{-S-Cys})_4]$ is also observed at low Cu^{I} stoichometries.[33] However, these clusters form in the inner core, as opposed to the outer core as observed

This article was published in the *Encyclopedia of Inorganic and Bioinorganic Chemistry* in 2021 by John Wiley & Sons, Ltd.
DOI: 10.1002/9781119951438.eibc2777

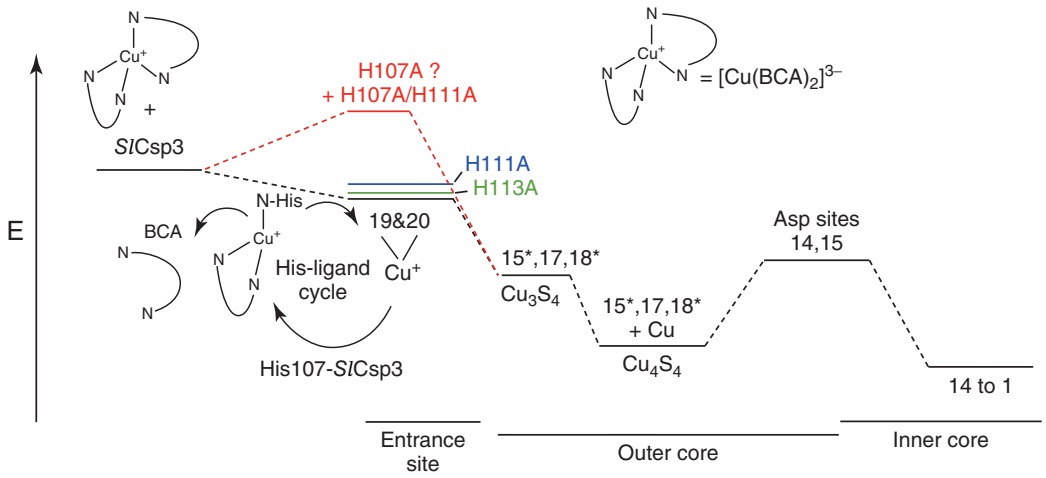

Figure 10 A model to account for the kinetic, structural, and site-directed mutagenesis data obtained for Cu^{I} loading to *Sl*Csp3 from the $[Cu(BCA)_2]^{3-}$ complex.[57] The relative stabilities of the copper sites are depicted relative to an arbitrary energy scale (*E*). [Straw, Megan L., Hough, Michael A., Wilson, Michael T., Worrall, Jonathan A.R. (2019). A histidine residue and a tetranuclear cuprousthiolate cluster dominate the copper loading landscape of a copper storage protein from Streptomyces lividans. *Chemistry – A European Journal*, **25**, 10678–10688.]

for *Sl*Csp3.[57] A reason for this difference is not immediately apparent, although it is noted that in *Mt*Csp3 the Asp residue found in *Sl*Csp3 at the interface between the outer and inner core is replaced with an Asn residue.[4] Thus, based on the Cu^{I} loading model reported for *Sl*Csp3, the absence of the negatively charged bidentate Asp residue in *Mt*Csp3 could remove the barrier to populating the inner core under low Cu^{I} stoichiometries. Regardless of these differences, a common theme appears in that the driving force to sequester Cu^{I} and prevent toxicity in Csp3 members is through initial formation of tetranuclear Cu^{I}–thiolate clusters.[33,57]

RELATED ARTICLES

Particulate Methane Monooxygenase; Methane Monooxygenase Hydroxylase; Ferritin; *b*-Type Cytochrome Electron Carriers: Cytochromes b_{562} and b_5, and Flavocytochrome b_2; Copper Transporters and Chaperones

REFERENCES

1 ML Straw, AK Chaplin, MA Hough, J Paps, VN Bavro, MT Wilson, E Vijgenboom and JAR Worrall, *Metallomics*, **10**, 180–93 (2018).

2 N Vita, S Platsaki, A Basle, SJ Allen, NG Paterson, AT Crombie, JC Murrell, KJ Waldron and C Dennison, *Nature*, **525**, 140–3 (2015).

3 C Dennison, S David and J Lee, *J Biol Chem*, **293**, 4616–27 (2018).

4 N Vita, G Landolfi, A Basle, S Platsaki, J Lee, KJ Waldron and C Dennison, *Sci Rep*, **6**, 39065 (2016).

5 S Sirajuddin and AC Rosenzweig, *Biochemistry*, **54**, 2283–94 (2015).

6 TJ Lawton and AC Rosenzweig, *J Am Chem Soc*, **138**, 9327–40 (2016).

7 SH Stanley, SD Prior, DJ Leak and H Dalton, *Biotechnol Lett*, **5**, 487–92 (1983).

8 RL Lieberman and AC Rosenzweig, *Nature*, **434**, 177–82 (2005).

9 R Balasubramanian, SM Smith, S Rawat, LA Yatsunyk, TL Stemmler and AC Rosenzweig, *Nature*, **465**, 115–9 (2010).

10 SY Ro, LF Schachner, CW Koo, R Purohit, JP Remis, GE Kenney, BW Liauw, PM Thomas, SM Patrie, NL Kelleher and AC Rosenzweig, *Nat Commun*, **10**, 2675 (2019).

11 MO Ross, F MacMillan, J Wang, A Nisthal, TJ Lawton, BD Olafson, SL Mayo, AC Rosenzweig and BM Hoffman, *Science*, **364**, 566–70 (2019).

12 AC Rosenzweig, CA Frederick, SJ Lippard and P Nordlund, *Nature*, **366**, 537–43 (1993).

13 JD Lipscomb, *Annu Rev Microbiol*, **48**, 371–99 (1994).

14 SD Prior and H Dalton, *J Gen Microbiol*, **131**, 155–63 (1985).

15 AK Nielsen, K Gerdes, H Degn and JC Murrell, *Microbiology*, **142**, 1289–96 (1996).

16 AK Nielsen, K Gerdes and JC Murrell, *Mol Microbiol*, **25**, 399–409 (1997).

17 GE Kenney, M Sadek and AC Rosenzweig, *Metallomics*, **8**, 931–40 (2016).

18 DW Choi, RC Kunz, ES Boyd, JD Semrau, WE Antholine, JI Han, JA Zahn, JM Boyd, AM de la Mora and AA DiSpirito, *J Bacteriol*, **185**, 5755–64 (2003).

19 M Martinho, DW Choi, AA Dispirito, WE Antholine, JD Semrau and E Münck, *J Am Chem Soc*, **129**, 15783–5 (2007).

20 R Balasubramanian and AC Rosenzweig, *Curr Opin Chem Biol*, **12**, 245–9 (2008).

This article was published in the *Encyclopedia of Inorganic and Bioinorganic Chemistry* in 2021 by John Wiley & Sons, Ltd.
DOI: 10.1002/9781119951438.eibc2777

21 GE Kenney and AC Rosenzweig, *ACS Chem Biol*, **7**, 260–8 (2012).

22 AA DiSpirito, JD Semrau, JC Murrell, WH Gallagher, C Dennison and S Vuilleumier, *Microbiol Mol Biol Rev*, **80**, 387–409 (2016).

23 C Dennison, *Chemistry*, **25**, 74–86 (2019).

24 JM Arguello, D Raimunda and T Padilla-Benavides, *Front Cell Infect Microbiol*, **3**, 73 (2013).

25 H Irving and RJP Williams, *Nature*, **162**, 746–7 (1948).

26 L Macomber and JA Imlay, *Proc Natl Acad Sci U S A*, **106**, 8344–9 (2009).

27 S Chillappagari, A Seubert, H Trip, OP Kuipers, MA Marahiel and M Miethke, *J Bacteriol*, **192**, 2512–24 (2010).

28 DK Fung, WY Lau, WT Chan and A Yan, *J Bacteriol*, **195**, 4556–68 (2013).

29 G Tan, Z Cheng, Y Pang, AP Landry, J Li, J Lu and H Ding, *Mol Microbiol*, **93**, 629–44 (2014).

30 C Rademacher and B Masepohl, *Microbiology*, **158**, 2451–64 (2012).

31 J Lee and C Dennison, *Int J Mol Sci*, **20**, 4144 (2019).

32 Z Xiao, PS Donnelly, M Zimmermann and AG Wedd, *Inorg Chem*, **47**, 4338–47 (2008).

33 A Basle, S Platsaki and C Dennison, *Angew Chem Int Ed*, **56**, 8697–700 (2017).

34 E Krissinel and K Henrick, *J Mol Biol*, **372**, 774–97 (2007).

35 DM Lawson, PJ Artymiuk, SJ Yewdall, JM Smith, JC Livingstone, A Treffry, A Luzzago, S Levi, P Arosio, G Cesareni, CD Thomas, WV Shaw and PM Harrison, *Nature*, **349**, 541–4 (1991).

36 FS Mathews, PH Bethge and EW Czerwinski, *J Biol Chem*, **254**, 1699–706 (1979).

37 KF Chater, *Philos Trans R Soc Lond Ser B Biol Sci*, **361**, 761–8 (2006).

38 Z Xiao and AG Wedd, *Nat Prod Rep*, **27**, 768–89 (2010).

39 P Bagchi, MT Morgan, J Bacsa and CJ Fahrni, *J Am Chem Soc*, **135**, 18549–59 (2013).

40 K Flardh and MJ Buttner, *Nat Rev Microbiol*, **7**, 36–49 (2009).

41 D Claessen, DE Rozen, OP Kuipers, L Sogaard-Andersen and GP van Wezel, *Nat Rev Microbiol*, **12**, 115–24 (2014).

42 GP van Wezel and KJ McDowall, *Nat Prod Rep*, **28**, 1311–33 (2011).

43 J Anne, B Maldonado, J Van Impe, L Van Mellaert and K Bernaerts, *J Biotechnol*, **158**, 159–67 (2012).

44 BJ Keijser, GP van Wezel, GW Canters, T Kieser and E Vijgenboom, *J Mol Microbiol Biotechnol*, **2**, 565–74 (2000).

45 JAR Worrall and E Vijgenboom, *Nat Prod Rep*, **27**, 742–56 (2010).

46 M Fujimoto, A Yamada, J Kurosawa, A Kawata, T Beppu, H Takano and K Ueda, *Microbiol Biotechnol*, **5**, 477–88 (2012).

47 KLM Blundell, MT Wilson, DA Svistunenko, E Vijgenboom and JAR Worrall, *Open Biol*, **3**, 12016 (2013).

48 KLM Blundell, MA Hough, E Vijgenboom and JAR Worrall, *Biochem J*, **459**, 525–38 (2014).

49 AK Chaplin, ML Petrus, G Mangiameli, MA Hough, DA Svistunenko, P Nicholls, D Claessen, E Vijgenboom and JAR Weorrall, *Biochem J*, **469**, 433–44 (2015).

50 ML Petrus, E Vijgenboom, AK Chaplin, JAR Worrall, GP van Wezel and D Claessen, *Open Biol*, **6**, 150149 (2016).

51 S Dwarakanath, AK Chaplin, MA Hough, S Rigali, E Vijgenboom and JAR Worrall, *J Biol Chem*, **287**, 17833–47 (2012).

52 AK Chaplin, BG Tan, E Vijgenboom and JAR Worrall, *Metallomics*, **7**, 145–55 (2015).

53 T Liu, A Ramesh, Z Ma, SK Ward, L Zhang, GN George, AM Talaat, JC Sacchettini and DP Giedroc, *Nat Chem Biol*, **3**, 60–8 (2007).

54 BG Tan, E Vijgenboom and JAR Worrall, *Nucleic Acids Res*, **42**, 1326–40 (2014).

55 GL Newton, N Buchmeier and RC Fahey, *Microbiol Mol Biol Rev*, **72**, 471–94 (2008).

56 L Banci, I Bertini, F Cantini, IC Felli, L Gonnelli, N Hadjiliadis, R Pierattelli, A Rosato and P Voulgaris, *Nat Chem Biol*, **2**, 367–8 (2006).

57 ML Straw, MA Hough, MT Wilson and JAR Worrall, *Chemistry*, **25**, 10678–88 (2019).

This article was published in the *Encyclopedia of Inorganic and Bioinorganic Chemistry* in 2021 by John Wiley & Sons, Ltd.
DOI: 10.1002/9781119951438.eibc2777